DOI: 10.1002/anie.200801605

Optics on the Nanoscale

Tip-Enhanced Near-Field Optical Microscopy

*Achim Hartschuh**

Keywords:
fluorescence spectroscopy · Raman spectroscopy · scanning probe microscopy · surface analysis

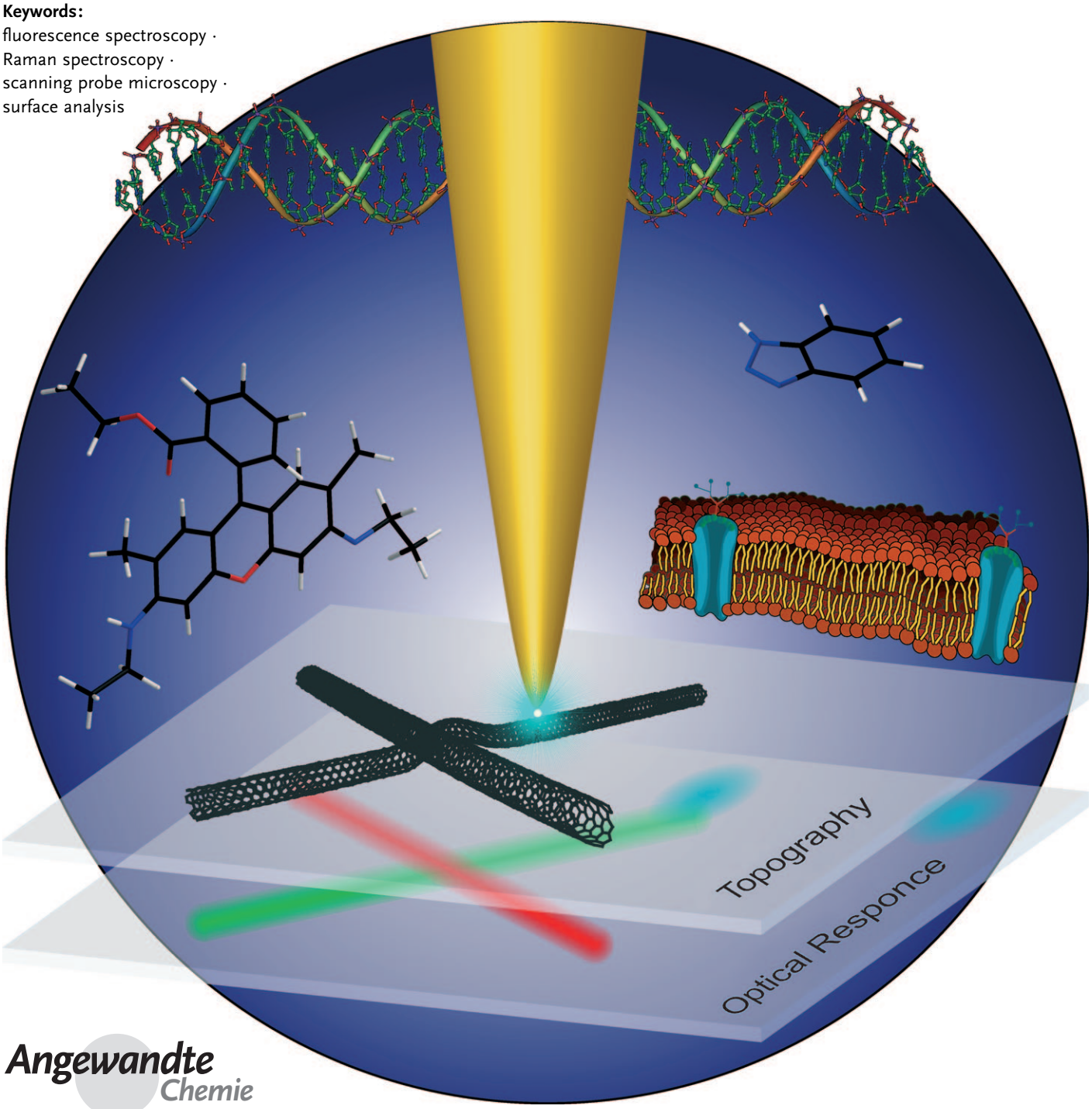

Spectroscopic methods with high spatial resolution are essential for understanding the physical and chemical properties of nanoscale materials, including quantum structures and biological surfaces. An optical technique is reviewed that relies on the enhanced electric fields in the proximity of a sharp, laser-irradiated metal tip. These fields are utilized for spatially confined probing of various optical signals, thus allowing for a detailed sample characterization far below the diffraction limit. In addition, tip-enhanced fields also provide the sensitivity crucial for the detection of nanoscale volumes. After outlining the principles of near-field optics, the mechanisms contributing to local field enhancement and how it can be used to enhance optical signals are discussed. Different experimental methods are presented and several recent examples of Raman and fluorescence microscopy with 10 nm spatial resolution of single molecules are reviewed.

From the Contents

1. Introduction

Optical microscopy forms the basis of most of the natural sciences. Life sciences, in particular, benefit from the fascinating possibility of studying the smallest structures and processes in living cells and tissue. Besides the direct visualization, structural-specific information crucial for chemical analysis is obtained through Raman spectroscopy. Optical techniques feature extremely high detection sensitivity, reaching the single-molecule limit in fluorescence, Raman, and absorption spectroscopy.[1–4] Today, our continuously increasing ability to control and structure nanoobjects has led to an urgent need for new microscopic tools—preferentially, optical microscopy with nanoscale spatial resolution. Moreover, novel measurement techniques always stimulate research in different areas by providing new insight and giving access to new physical phenomena.

Optical diffraction is a function of the wave nature of light. The spatial resolution of conventional microscopy is limited to half the wavelength of the light used. In the last decade optical microscopy has been extended down to nanometer length scales through the development of far-field and near-field techniques. Far-field techniques rely on the detection of propagating waves at distances from the source that are larger than the wavelength of the electromagnetic wave, while near-field techniques exploit short-range evanescent waves. Near-field optical microscopy, initiated by pioneering work of Pohl, Lewis, and others in the 1980s, raised high expectations for the first resolution at the nanoscale.[5,6] The history of near-field optics is reviewed in recent articles by Pohl and Novotny.[7,8] In addition, numerous reviews and books describe the fundamentals and applications of near-field optics.[9–12] This Review focuses on recent developments of a particular type of near-field technique that is based on a laser-illuminated metal tip. This technique, which is termed tip-enhanced near-field optical microscopy (TENOM), has been shown to be the most powerful tool for the optical characterization of surfaces, not only providing superior spatial resolution down to 10 nm but also enormous signal enhancement.

The basic physical principles of evanescent and propagating waves as well as the loss of spatial information upon propagation are first outlined. In the following sections the origin of electromagnetic field enhancement at a metal tip and applications for signal enhancement are described. Experimental transformations and recent examples of tip-enhanced Raman scattering and fluorescence are reviewed. The outlook addresses future prospects of TENOM and the remaining challenges.

2. Principles

The goal of near-field optics is to overcome the diffraction limit of optical imaging.[13,14] In the following the physical principles underlying the diffraction limit that is associated with the optical far-field formed by propagating waves are outlined and their evanescent counterpart that dominates the near-field of a radiation sourceis described. A powerful tool for describing wave propagation is the so-called angular spectrum representation. Here, the electric field $\boldsymbol{E}$ in the detector plane at z is expressed as the superposition of harmonic waves of the form $\exp(i\boldsymbol{kr}-i\omega t)$ with amplitudes $\tilde{\boldsymbol{E}}(k_x,k_y,z=0)$ that emanate from the source plane at $z=0$ [Eq. (1)].[15,9]

[*] Prof. Dr. A. Hartschuh
Department Chemie und Biochemie and CeNS
Ludwig-Maximilians-Universität München
Butenandtstrasse 5–13 E, 81377 München (Germany)
Fax: (+89) 2180-77188
E-mail: achim.hartschuh@cup.uni-muenchen.de
Homepage: http://www.cup.uni-muenchen.de/pc/hartschuh

$$\boldsymbol{E}(x,y,z) = \int_{-\infty}^{+\infty} \int \bar{\boldsymbol{E}}(k_x,k_y,z=0)\mathrm{e}^{i(k_x x+k_y y)}\mathrm{e}^{\pm i k_z z}\mathrm{d}k_x\,\mathrm{d}k_y \qquad (1)$$

The wave vector $\boldsymbol{k}$, which describes the propagation direction of the wave, is represented by its components $\boldsymbol{k}=(k_x,k_y,k_z)$, while its length is fixed by the wavelength of the light λ and the refractive index of the medium n through $|\boldsymbol{k}| = \sqrt{k_x^2+k_y^2+k_z^2} = 2\pi n/\lambda$. In Equation (1) the time dependence of the fields has been omitted for clarity. For simplicity the following discussion is limited to the x-z plane and $n=1$ such that $|k_z| = \sqrt{2\pi^2/\lambda^2 - k_x^2}$. In Equation (1) the term $\exp(\pm i k_z z)$ controls the propagation of the associated wave: For $k_x \le 2\pi/\lambda$, the component k_z is real and the corresponding wave with amplitude $\bar{\boldsymbol{E}}(k_x,z=0)$ propagates in the z direction with an oscillation of $\exp(-i k_z z)$. If $k_x > 2\pi/\lambda$, the component k_z becomes complex and $\exp(-|k_z|z)$ describes the exponential decay of the associated, and therefore, evanescent wave. As a result, only waves with $k_x \le 2\pi/\lambda$ can propagate and contribute to the field far from the source. Figure 1 illustrates this behavior: On the left the electric field $\boldsymbol{E}$ emanating from a narrow subwavelength source is shown together with its angular spectrum calculated by the inverse of Equation (1). In general, the wave amplitudes $\bar{\boldsymbol{E}}$ result from a two-dimensional Fourier-transformation of $\boldsymbol{E}$. As for the correlation between the time and the frequency domain, where a short optical pulse requires a broad frequency spectrum, a sharp field distribution requires a broad spectrum of spatial frequencies k_x. Since only waves with spatial frequencies limited to $k_x \le 2\pi/\lambda$ can propagate, the spectral width rapidly decreases with increasing distance from the source z, thereby leading to a fast broadening of the electric field distribution in real space. In other words, propagation corresponds to low-pass filtering with a frequency limit $k_{x,\max} = 2\pi/\lambda$. The far-field thus contains limited spatial frequencies equivalent to limited spatial information. To overcome this limitation, both far-field and near-field concepts have been developed that are outlined in the following section.

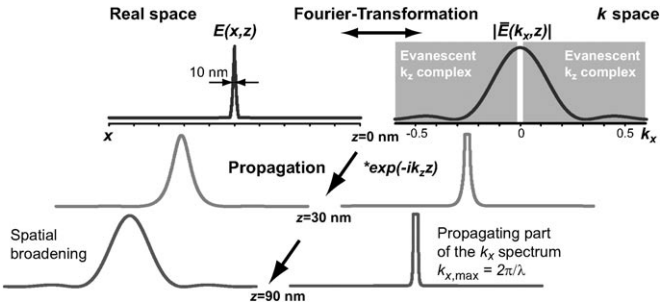

Figure 1. Schematic representation illustrating the propagation of waves and the loss of spatial information. Top row: Initial field distribution $\boldsymbol{E}(x,z=0)$ at a 10 nm wide source in the x-z plane (left) and corresponding angular spectrum $|\bar{\boldsymbol{E}}(k_x,z=0)|$ (right). The spectrum contains both evanescent and propagating waves near the source. The two lower rows illustrate the development of the fields at a distance of $z=30$ nm and $z=90$ nm. Only waves with $k_x \le 2\pi/\lambda \approx 0.0126\ \mathrm{nm}^{-1}$ propagate when light with a wavelength of $\lambda=500$ nm is used in a vacuum. Evanescent waves decay exponentially following $\exp(-k_z z)$. The decay of high spatial frequencies leads to spatial broadening and loss of spatial information.

Achim Hartschuh studied Physics at the universities of Tübingen and Stuttgart, Germany, and received his PhD in 2001 with Prof. H. C. Wolf. He spent two years carrying out postdoctoral research at the Institute of Optics at the University of Rochester, New York, USA, in the research group of Prof. L. Novotny. In 2002 he became Junior Professor at the University of Siegen and moved after two years to the University of Tübingen. Since 2006 he has been Professor at the LMU München, Germany.

2.1. Far-Field Concepts

Signals emanating from two identical incoherent sources separated by a few tens of nanometers only (for example, two fluorescent molecules) cannot be distinguished in the far-field since high spatial frequencies containing the necessary information are lost upon wave propagation. To distinguish the signals from the two sources, far-field techniques require situations in which the two sources do not emit simultaneously at all times with the same emission properties. This situation can be achieved either by active control, for example, through stimulated emission depletion (STED),[16,17] or by using stochastical readouts based on photophysical and photochemical effects of the source, such as photoinduced blinking, bleaching, or switching. The latter approaches are termed photoactivated localization microscopy (PALM) and stochastic optical reconstruction microscopy (STORM).[18,19] The STORM and PALM methods rely on a high signal to noise ratio, which is determined mainly by the detection sensitivity and fluorescence quantum yield which needs to be sufficient to discriminate the signal from single emitters. In this case, the problem of spatial resolution is reduced to the problem of position accuracy that describes the task of localizing a single emitter. Optimized techniques currently reach a position accuracy of about 1.5 nm for single molecules.[20] When fluorescent markers are used to visualize sample structures, the spatial separation of the markers needs to be on the length scale of the desired spatial resolution in the sample, for example, at corresponding high concentrations of approximately 1 marker in 10 nm^3.

A recent review on the principles, progress, and prospects of high-resolution far-field techniques is given in Ref. [21] In general, existing far-field concepts rely on the photophysical or photochemical properties, such as emission energy or excited-state lifetime, of the sample and thus require prior knowledge. A great advantage of these techniques is their three-dimensional imaging capability—a prerequisite for intracellular studies.[22] On the other hand, existing far-field techniques do not provide signal enhancement, which becomes increasingly relevant upon further decrease in the detection volume. At present, existing far-field techniques are not applicable to Raman scattering.

2.2. Near-Field Concepts

Near-field optical microscopy follows a different approach, in which high spatial information is achieved through interactions between a pointed probe and the electromagnetic near-field of the sample. Raster scanning the probe and simultaneous signal detection then allows for image formation. Since higher spatial frequencies are associated with faster exponential decay (see definition of k_z in Section 2), high-resolution imaging requires probe–sample distances of a few nanometers. As a consequence, near-field microscopy is limited to surface or subsurface studies.[23]

Four different focusing concepts are illustrated in Figure 2, including lens-based far-field focusing (Figure 2a), the widely used aperture-type approach (aperture-SNOM, Figure 2b), and tip enhancement (Figure 2c and d), which is the focus of this Review.

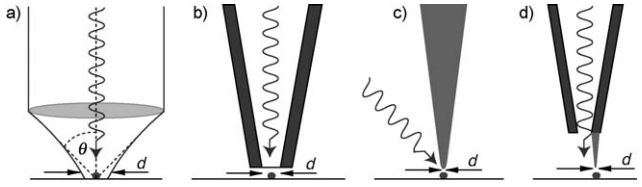

Figure 2. Focusing concepts: a) Far-field focusing using a lens. The angular frequency range of propagating waves $k_{x,max}$, and thus the focus diameter, is limited by the aperture angle of the lens $k_{x,max} = n \sin(\theta) 2\pi/\lambda$, with n being the refractive index and λ the wavelength of light. b) Aperture-type scanning near-field optical microscope (aperture-SNOM). c) Tip-enhanced near-field optical microscopy (TENOM). d) Tip-on-aperture (TOA) approach, which combines the advantages of (b) and (c).

The introduction of the aperture probe in the 1980s for near-field microscopy allowed, for the first time, optical imaging with a resolution better than the diffraction limit, and stimulated interest in many disciplines, especially the material and biological sciences.[8,24,25] Aperture probes typically consist of an aluminum-coated fiber tip, the end of which is left uncoated to form a small aperture. Unfortunately, only a tiny fraction ($\leq 10^{-4}$ for a 100 nm aperture) of the light coupled in the fiber is emitted at the aperture, because the propagating waveguide modes are effectively cut-off as the diameter of the tip becomes smaller.[26] In tip-enhanced near-field optical microscopy (TENOM), enhanced optical fields in proximity to a sharp metallic probe are used to locally excite the sample and to extract the emitted light (Figure 2c). Figure 2d shows the so called tip-on aperture (TOA) probe that combines the advantages of the aperture type and TENOM. The use of laser-illuminated metal tips for near-field imaging was suggested by Wessel in 1985.[27] In general, three different approaches can be distinguished: 1) Scattering-type microscopy in which the sample response is detected in the far-field at the frequency of the incident light;[28–30] 2) tip-enhanced nonlinear optical frequency generation and mixing, such as, for example, through second-harmonic generation (SHG) and four-wave mixing (4WM);[10,31–34] 3) tip-enhanced microscopy, which utilizes the locally enhanced fields to increase the inelastic spectroscopic response of the system.[1,10,11,35–37] Local signal enhancement serves to achieve high spatial resolution, but also increases the detection sensitivity enormously. The technique is, therefore, applicable to weak emitters with low quantum yields or intrinsically weak signals such as Raman scattering. The versatility of the technique allows the study of a variety of spectroscopic signals, including local time-resolved fluorescence. This Review focuses on the third approach and the interested reader is referred to the references listed for the other two approaches. The next section of this Review contains a brief theoretical description of field enhancement at a metal tip and how these fields modify the optical signals.

3. Field-Enhancement at a Metal Tip

Field enhancement at metal structures is a phenomenon we encounter almost daily, as it forms the principle of a lightning rod, a radio antenna, and the coloring based on metallic nanoparticles. In fact, the three examples also illustrate the different contributions to field enhancement: The electrostatic lightning-rod effect is caused by geometric singularities that lead to highly localized surface-charge densities, which also form the basis for field emission (Figure 3a). Surface plasmon resonances of metal particles reflect the shape and dielectric properties and result in characteristic extinction spectra (Figure 3b). Antenna resonances become relevant if the length of the metal structure matches multiples of half the wavelength of the radiation (Figure 3c and d).[38,39] Antenna and plasmon resonances exhibit distinct wavelength dependencies, with pronounced maxima in the field intensity that are tunable through the visible spectral range. The electrostatic lightning-rod effect depends on the conductivity of the material at light frequencies, and typically increases towards the IR spectral range.[38,40]

Numerous theoretical studies have been published in which a variety of techniques have been employed to quantify the contributions from different field-enhancement mechanisms and to find the optimum tip structure. The difficulty in characterizing metallic structures in the optical regime results from the fact that metals do not behave as perfect conductors at these frequencies. Electromagnetic fields are not confined to surfaces, and their finite depth ultimately results in deviations from simple antenna theory. Another consequence is the formation of surface plasmon polaritons at the boundary between metals and dielectrics. The influence of the tip shape and material on the field enhancement has been discussed in a series of publications aimed at finding the optimum tip.[41–43] For simple tip structures, the highest enhancement is predicted theoretically and verified experimentally to occur in the retarded regime, that is, when the antenna length is related to an effective wavelength.[39,44] Results from different numerical techniques need to be compared quantitatively to assess the technical difficulties and to maximize the significance of theoretical predictions.[45]

Theory and experiments on surface-enhanced Raman scattering show that the highest enhancement results with two

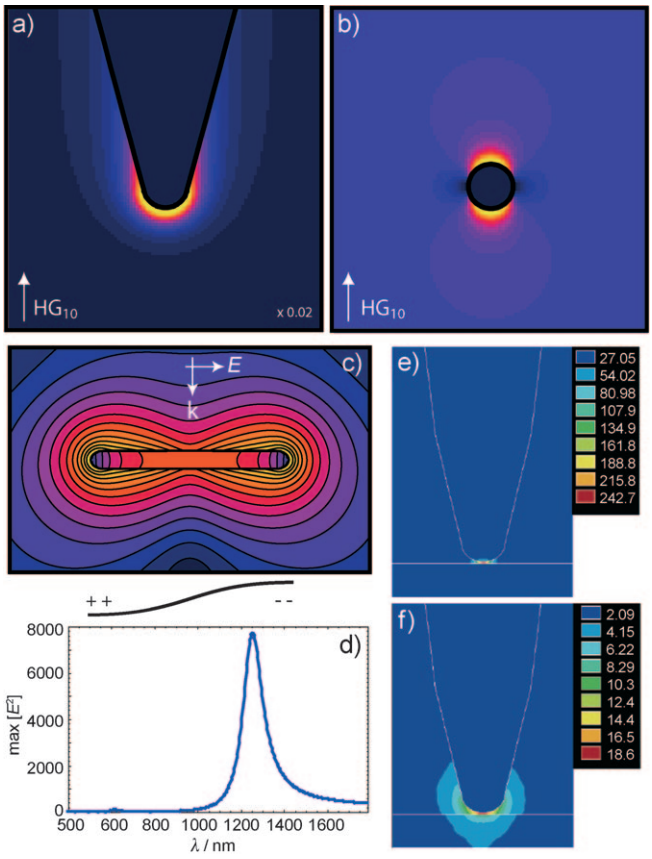

Figure 3. Field enhancement at nanostructures results from three different contributions: 1) The quasistatic lightning-rod effect requires a geometric singularity and is observable for semi-infinite pointed probes. 2) Surface plasmon resonances result from collective excitations of electrons that reflect both the shape and dielectric properties of metal particles. a) and b) present calculated field distributions $|E_{local}(\mathbf{r},\omega)|^2$ near a gold tip (a) and a sphere (b) located above a glass substrate and irradiated by an on-axis-focused HG_{10} laser mode. Reprinted from Ref. [86], Copyright 2006, with permission from *Annual Reviews*. 3) Antenna resonances occur when the tip length is related to an effective wavelength ((c) and (d)). Reprinted from Ref. [8], Copyright 2007, with permission from Elsevier. Electric-field enhancement and confinement at a metal tip is strongly increased for metallic substrates (e) compared to glass substrates (f). Reprinted from Ref. [53], Copyright 2005, with permission from the American Chemical Society.

or more particle configurations, such as through the combination of spheres, antennas, or in more complex colloidal aggregates.[34,44,46–52] Similarly, field enhancement is increased enormously by combining tips over metal surfaces with higher localization (Figure 3 e,f).[53–56] In contrast, field enhancement is expected to drop rapidly for samples covered by a thin dielectric layer.[23] The interaction between the tip and the sample substrate leads to surface- and distance-dependent spectral shifts of the plasmon resonances which complicate the quantification of the field enhancement achieved in a particular configuration.[57–60]

Recent experiments using tips on metallic substrates revealed that fields are enhanced additionally by surface features of sub- or a few nanometer sizes, which are hard to observe in AFM images (see also Figure 9 in Section 7).[60,61] To avoid artefacts, atomically smooth metal substrates are necessary for quantitative TENOM imaging. Maximized fields are not sufficient for TENOM applications since they also have to be accessible in the scanning probe configuration, and therefore have to occur at the extremities of the particle or tip.[39] Moreover, the dimensions of the probe should be small, since they directly determine the topographic resolution and the possibility of topographic artefacts resulting from variations in the tip–sample distance.[62,63]

The field distribution and localized enhancement do not only depend on the particle arrangement and wavelength but also on the polarization state of the excitation light. To establish a strong field enhancement at tips formed by sharpened wires, the electric field of the exciting laser beam needs to be polarized along the tip axis.[38] Initially, field distributions were calculated for continuous excitation with plane waves. In the retarded regime, where light propagation becomes relevant—such as in the case of extended antenna structures—tightly focused excitation or excitation with evanescent waves will lead to modified field distributions. Advanced approaches for field engineering utilize surface plasmon propagation and retardation. Chirp- and polarization-controlled laser pulses can be designed so that the targeted adaptive subwavelength control of nanooptical fields at metal structures can be achieved. This has recently been developed into an efficient tool that has resulted in the new field of ultrafast nanooptics.[64–67] An important step is the development of nonoptical techniques for the visualization of fields and electromagnetic eigenmodes of nanostructures. The combination of electron energy loss spectroscopy (EELS) and scanning transmission electron microscopy (STEM) can be applied to observe plasmons as resonance bands in the energy-loss spectra of focused electron beams, thus providing nanometer spatial resolution.[69] Energy-resolving two-photon photoemission electron microscopy (PEEM) probes the electric-field potential with the spatial resolution of 0.5 nm determined by the electron optics.[66,67]

4. Enhancement of Optical Signals with a Metal Tip

Although the enhanced electromagnetic fields are localized at the tip apex (see previous section and Figure 3), the image contrast formed by raster scanning the sample does not simply reflect the tip shape. In other words, tip-enhanced optical imaging does not correspond to atomic force microscopy (AFM) with optical information. In particular, since Raman scattering and fluorescence are distinct optical processes involving different electronic states of the sample material with a different degree of coherence, the enhancement effects for either type of sample, and thus the image contrast, is expected to vary.

The enhanced fields at the tip cause enhanced excitation rates that correspond to an increase in the excitation density provided by the light source. In general, the enhancement of the excitation rate k_{ex} will be identical for Raman scattering and fluorescence if the electronic dephasing is not changed. By defining the field enhancement factor f as the ratio

between the electric field at the tip $E_{tip}(x)$ and without the tip $E_0(x)$, the excitation rate enhancement is expressed as $k_{ex,tip}/k_{ex,0} = f^2$. In analogy to a radio which can be used both as a receiver and a sender, the enhanced fields can also promote radiative decay, which is expressed by the rate k_{rad}. This enhancement of the radiative rate can be explained in terms of the Purcell effect and is expressed by Fermi's golden rule in the weak coupling range.[70,71]

4.1. Enhancement of Raman Scattering

In the case of Raman scattering, the total signal depends on the product of the transition rates $k_{ex}(\lambda_{ex})k_{rad}(\lambda_{rad})$. As a consequence, the total signal enhancement scales with the fourth power of the field enhancement for small differences between the excitation and emission wavelength, assuming that the field enhancement at the tip does not depend sensitively on the wavelength [Eq. (2)].

$$M_{Raman} = (k_{ex,tip}/k_{ex,0})\,(k_{rad,tip}/k_{rad,0}) \approx f^4 \quad (2)$$

For the general case of surface-enhanced Raman scattering (SERS), enhancement factors of up to 12 orders of magnitude have been reported for particular multiple particle arrangements with interstitial sites between the particles or sharp protrusions on the outside surface.[46,72] Since the signal scales with the fourth power, a moderate field enhancement, predicted for a single spherical particle to be in the range of $f = 10$–100, is already sufficient for enormous signal enhancement.

4.2. Enhancement of Fluorescence

The fluorescence intensity depends on the excitation rate k_{ex} and the quantum yield η, which denotes the fraction of transitions from the excited to the ground state that give rise to an emitted photon. The quantum yield is expressed in terms of the radiative rate k_{rad} and the nonradiative rate k_{nonrad} through $\eta = k_{rad}/(k_{rad} + k_{nonrad})$. Accordingly, the fluorescence enhancement arising from the presence of the metal tip can be written as Equation (3).

$$M_{flu} = (E_{tip}/E_0)^2(\eta_{tip}/\eta_0) = f^2(\eta_{tip}/\eta_0) \quad (3)$$

Here, we assume that the system is excited far from saturation. From Equation (3) it is clear that TENOM works most efficiently for samples with a small fluorescence quantum yield and fast cycling rates, such as, for example, with semiconducting single-walled carbon nanotubes.[73,74] For highly fluorescent samples, such as dye molecules, the quantum yield η_0 is already close to unity and cannot be enhanced further. The small separation between the emitter and the metal tip that is required for high spatial resolution (below 10 nm in typical experiments) necessitates that nonradiative transfer of energy from the electronically excited molecule to the metal followed by nonradiative dissipation in the metal has to be taken into account. This process represents an additional nonradiative relaxation channel and reduces the number of detected fluorescence photons. Although the theory of energy transfer between molecules and flat metal interfaces is well understood in the framework of phenomenological classical theory,[75,76] nanometer-sized objects are more difficult to quantify. The tip-induced enhancement and quenching of the radiative rate has been studied theoretically.[51,71,77–80] Experiments on model systems comprised of single dipole emitters such as fluorescent molecules and metal particle antennas revealed a distance-dependent interplay between competing enhancement and quenching processes.[81–85] Besides amplifying the emission signals, the particle-induced enhancement of the radiative rate can also lead to a substantial spatial and spectral redistribution of the emission.[83,86,87] The orientation of the emitter dipole with respect to the antenna structure is of major importance for the resulting modification of the radiative rate.[83] Although semiconducting tips will result in less-efficient quenching,[88,89] they will also provide weaker enhancement because of their lower conductivity at optical frequencies.

Since signal enhancement and high spatial resolution are the result of near-field interactions between the probe and sample, TENOM spectra can differ substantially from the corresponding far-field spectra. Large wave vectors $\boldsymbol{k}$, for example, are expected to initiate optical transitions beyond standard dipole approximations, assuming constant excitation fields.[90–92] Large field gradients could influence the selection rules, thus leading to different Raman spectra.[93] An improved understanding of near-field optical interactions and phenomena would enable their controlled exploitation, thus leading to additional and new spectroscopic information.

5. Experimental Realizations

5.1. Near-Field Microscopes

Since field enhancement is localized at the tip apex, methods to control the tip–sample distance on the length scale of a few nanometers are required. Experimental implementations are based on the detection of normal or shear forces in AFM or the detection of current in scanning-tunneling microscopy (STM).[94,95] A variety of TENOM probes are employed, including sharp gold or silver tips fabricated by electrochemical etching of thin wires and metal-coated AFM probes, which are commercially available.[10,35,37] Alternatively, field-enhancing metal particles can be attached to sharpened glass probes.[96–98] More elaborate approaches combine etching and focused ion beam milling (FIB) to give tailored plasmonic structures, such as the so-called bow-tie antennas.[81,99,100]

Illumination methods can be divided into two classes based on their applicability to nontransparent samples (Figure 4). Side illumination allows the study of nontransparent samples, for which the required polarization along the tip axis can be easily fulfilled (Figure 4b). In the case of transparent samples, on-axis illumination can benefit from high numerical aperture objectives (NA > 1) that decrease

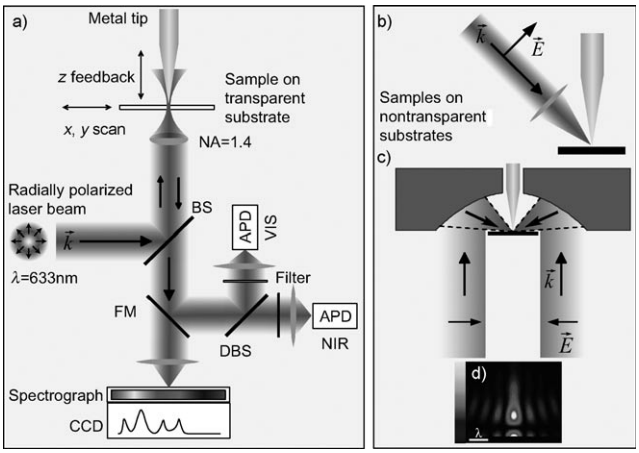

Figure 4. a) Schematic representation of a near-field microscope with on-axis illumination of the tip through a transparent sample.[73] The optical signal is detected either by two avalanche photodiodes (APDs) for the VIS and NIR ranges or by a combination of a spectrograph and a CCD camera. b) Side-illumination of the tip on top of a nontransparent substrate. c) Focusing of light using a parabolic mirror. To generate a strong field component parallel to the tip axis required for efficient field enhancement, (a) and (c) utilize a radially polarized laser mode.[60,101,102] d) Calculated field distribution of a focused radially polarized beam. Reprinted from Ref. [60].

the size of the confocal volume contributing to the far-field background and that maximize the collection efficiency of the emitted light. The later point is paramount in the case of weakly fluorescent species, for which photobleaching at high excitation densities becomes an issue. For on-axis illumination, however, light propagation is parallel to the polarization direction required for efficient field enhancement at the tip. This requirement can be fulfilled by using higher order laser modes.[101,102] Nontransparent samples can be investigated at high numerical aperture by employing parabolic mirror objectives instead of glass objectives (Figure 4c).[60,103,104] Moreover, parabolic mirrors do not exhibit chromatic aberrations and can be used at all temperatures as well as under UHV conditions, thus making them ideally suited for surface-science studies. Their alignment is delicate, since minor deviations already lead to substantially altered focal fields and reduced detection sensitivity.[103]

To acquire an image, the tip is positioned in the focus of the objective and illuminated by laser light. The optical signal is typically collected through the same objective and detected either using sensitive photodiodes or spectrometers equipped with CCD cameras. Raster scanning the sample then allows for the simultaneous detection of near-field optical signals and the topography of the sample. Spectroscopic images formed by acquiring spectra at each pixel of the scan provide very detailed information and offers true spectroscopic contrast.

5.2. Far-Field Background

The configurations discussed so far utilize far-field illumination of the metal tip. As mentioned above, besides the signal resulting from the near-field interaction between the tip and the sample, a far-field signal is detected, which is referred to as the far-field background. A substantial near-field enhancement of the signal is thus necessary since it needs to compete with the far-field background resulting from the much larger diffraction-limited sample volume. For high-resolution imaging, the signal results approximately from a circular sample surface area of $\pi(5\,\mathrm{nm})^2$, whereas the confocal area is about $\pi(200\,\mathrm{nm})^2$. These values lead to a surface area ratio of 40000/25. In bulk samples, the finite decay length of the near-field of about 10 nm and the longitudinal focal depth of about 500 nm in far-field microscopy must be taken into consideration; this further increases the ratio by a factor of 50. From this viewpoint it is apparent that TENOM works best for low-dimensional structures such as 1D nanowires or isolated emitters such as semiconductor quantum dots.

Several approaches to minimize or delineate the background contribution have been developed. One such approach makes use of the rapid decay of the near-field signal upon increasing the tip–sample distance. Here, tapping-mode AFM is used to probe the sample while the optical signal is demodulated at the fundamental or higher harmonics of the tapping-mode frequency. This approach also forms the basis of elastic scattering microscopy mentioned previously in Section 2. In the case of weakly emitting samples, such as with single fluorescent molecules, the detection time (time tagging) of the photons with respect to the tapping oscillation is used. In this way, photons related to dominating near-field interactions and generated in small tip–sample distances can be distinguished from those corresponding to far-field contributions at larger tip–sample distances.[55,105] The corresponding demodulation of CCD signals is currently challenging, and precludes the acquisition of complete spectra at higher harmonic tapping mode frequencies.

Different approaches utilize particular probes that avoid far-field excitation of the sample area. The so-called tip-on-aperture (TOA, Figure 2) combines the best of two techniques: high spatial resolution and signal enhancement provided by sharp tips and illumination of the tip with an evanescent wave resulting from an aperture smaller than the wavelength.[106,107] In addition, tip fabrication allows the tip length to be tuned to match the antenna resonances, thereby further maximizing the field enhancement.[108] Other methods make use of surface plasmon propagation. The challenge of coupling propagating light to plasmons can be met through the coupling of the grating to the light. In such an approach, laser excitation of a grating written by FIB into a tapered gold tip is used to launch surface plasmons that propagate to the tip apex.[109] Efficient excitation of propagating plasmons can also be achieved by using higher order laser modes coupled into opaque metal-coated tapered glass fibers.[79,110,111]

In a simplified view, a tip-enhanced near-field optical microscope is built by combining a confocal microscope with a setup for controlling the tip–sample distance, for example, an atomic force (AFM) or a scanning tunneling microscope (STM). Although these microscopy techniques are fully developed, their combination certainly adds substantial complexity and will require careful design modifications to

achieve a high-degree of user-friendliness. Although there is a huge variety of different probes for AFM, including chemically functionalized and magnetic probes, most of the commercially available tips to date can not be used efficiently for TENOM, as they are based on semiconductor materials that provide only weak signal enhancement (see Section 4). The large-scale fabrication of metallic or metallized probes with maximized field-enhancement factors at high reproducibility is a key issue at present.

6. Tip-Enhanced Fluorescence (TEF)

Confocal microscopes offer detection efficiencies sufficient for the fluorescence imaging of single molecules with high fluorescence quantum yield. Here, the signal enhancement provided by the tip serves mainly to increase the spatial resolution. There are many examples in the literature of tip-enhanced fluorescence microscopy that use one- or two-photon excitation.[1,73,82,83,105,107,108,112,113] In the following, selected examples are reviewed to highlight the capabilities of TENOM and to illustrate the discussions in the previous sections.

6.1. Single-Molecule Fluorescence Enhancement

Several experiments demonstrate the competition between field-enhancement and tip-induced quenching in clearly defined single-molecule experiments (see also Section 4). Metallic spheres have been used, for which the field distribution can be calculated analytically.[82–84,107,114]

Figure 5a shows the dependence of the fluorescence signal on the distance for a single molecule oriented perpendicular to the substrate plane. Substantial signal enhancement is observed upon decreasing the tip–sample distance, while fluorescence quenching is observed to dominate below about 5 nm. The good agreement between the theoretical and experimental curves, including different dipole orientations with respect to the tip, indicate that this effect is well understood and can be accounted for in experiments.[82,83,115] As a result of the different distance dependencies for fluorescence enhancement and quenching, there is an optimum tip–sample distance in tip-enhanced fluorescence microscopy (see Figure 5a and Section 4.2). Several experiments have been carried out in which additional inert polymer layers were used as spacers to ensure the spacing.[108,116] However, as shown in Ref. [23], this results in a substantial loss in field enhancement and resolution because of the drop in field strength caused by the dielectric.

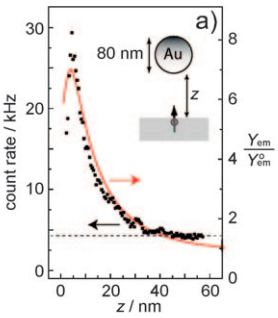

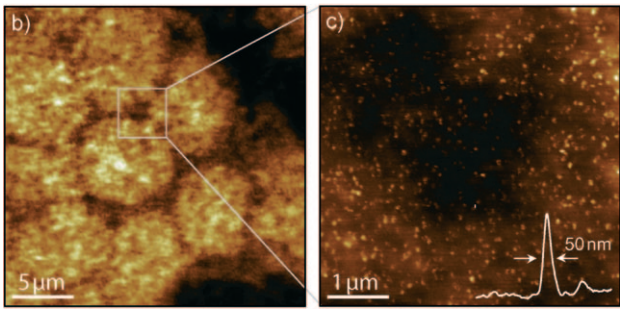

Figure 5. a) Distance dependence of the fluorescence enhancement of a single dye molecule provided by a 80 nm gold nanoparticle antenna. The red curve displays the theoretically expected enhancement. Reprinted from Ref. [82], Copyright 2006, with permission from the American Physical Society. b) Confocal fluorescence image of individual erythrocyte plasma membranes in aqueous buffer solution. c) Near-field fluorescence image of the area marked in (b), in which individual PMCA4 proteins are resolved. The image was acquired with a 60 nm gold nanoparticle antenna. The inset shows a cross-section through one of the fluorescence spots and a resolution of 50 nm. Reprinted from Ref. [117], Copyright 2008, with permission from the American Chemical Society.

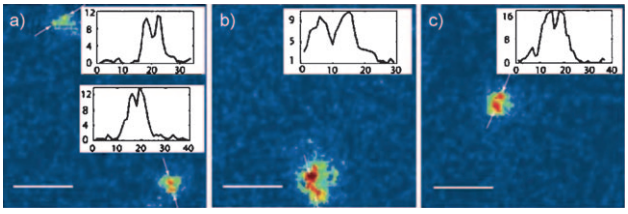

Figure 6. a)–c) Near-field images of Cy3 pairs on a surface. The insets show the profiles along the line cut through the image centers (indicated by arrows). The horizontal axis is in pixels (1 pixel = 1.95 nm) and the vertical axis is the pixel signal. Scale bars: 50 nm. Reprinted from Ref. [105], Copyright 2006, with permission from the American Physical Society.

6.2. Imaging of Fluorescent Biosurfaces

The applicability of TENOM to the fluorescence imaging of biological surfaces in aqueous buffer solution has been demonstrated recently.[117] Figure 5c shows near-field fluorescence images of erythrocyte plasma membrane immersed in water with a spatial resolution of about 50 nm. Figure 6 presents fluorescence images of single Cy3 dye molecules covalently bound to the termini of short DNA strands.[105] In this example, efficient far-field background suppression was achieved by time-tagging each detected photon followed by optimized temporal filtering (see Section 5). Dye molecules spaced less than 10 nm apart are resolved with high signal to noise ratio. Since spectra from highly sensitive CCD cameras can not at present be demodulated at typical tapping mode frequencies in the range of 100 kHz, time-tagging of photons comes at the cost of reduced spectral information. Images acquired with a TOA probe of dye-labeled DNA have been

presented in Ref. [107]. Besides providing high spatial resolution, the radially symmetric field distribution at the tip allows the 3D orientation of the transition dipole moment to be visualized. Since the sample is not excited in the far-field, this approach minimizes the far-field background and simultaneously reduces the irreversible bleaching of the fluorescence.[107,108]

Besides the imaging of fluorescent molecules typically used for the labeling of biological structures, TENOM is particularly well suited to the investigation of the photoluminescence (PL) of semiconducting single-walled carbon nanotubes (SWNTs). SWNTs are photoluminescent quasi-one-dimensional systems with great promise for applications in photonics as well as opto- and nanoelectronics.[118] A rapidly increasing number of studies demonstrate their enormous potential as luminescent markers in biological studies. The emission in the near-infrared spectral region, in which no autofluorescence occurs, is a great advantage.[119] The luminescence efficiency of nanotubes currently varies between a few percent to 10^{-4}; the reason for this is the efficient nonradiative decay caused by defects and coupling to intrinsic non-emissive dark states.[120–124] Although many fundamental properties have been discovered and explained recently, open questions remain, such as the role of local environmental perturbations and interactions between nanotubes. Tip-enhanced fluorescence microscopy has been shown to be well-suited to visualize and study such phenomena along single nanotubes.[73,125]

Figure 7a shows the photoluminescence image of nanotubes in the region from 860 nm to 1050 nm. The PL signals are extended along the entire nanotubes, although with different intensities. Energy-resolved images revealed that the extended structure is in fact a thin nanotube bundle comprising a (9,1) and a (6,5) nanotube.[125] The localizing of the two nanotubes simultaneously in the corresponding spectroscopic images with subnanometer precision allowed for the quantification of the distance dependence of the near-field-mediated energy transfer between the two adjacent nanotubes for the first time.[125] Simultaneous near-field Raman and PL imaging of nanotubes is possible and can be used to compare the different enhancement mechanisms.[73,126] The observed signal enhancement is typically stronger in the case of PL. This is somewhat surprising since the Raman signal scales with the fourth power of the field-enhancement factor, whereas the PL signal is expected to scale only quadratically. Equations (2) and (3) indicate that $M_{Flu} > M_{Raman}$ is only possible if $(\eta_{tip}/\eta_0) \geq 1$. As the quantum yield cannot be larger than unity, $M_{Flu} > M_{Raman}$ requires an intrinsic quantum yield that is very small ($\eta_0 \ll 1$), as for SWNTs. Since the nonradiative rate k_{nonrad} is not expected to be decreased by the tip, an increased quantum yield requires substantial enhancement of the radiative rate k_{rad} in the presence of the metal tip, as discussed in Section 4. These results demonstrate that tip-enhanced fluorescence microscopy is particularly promising for the fluorescence imaging of weakly emissive (bio-)surfaces.

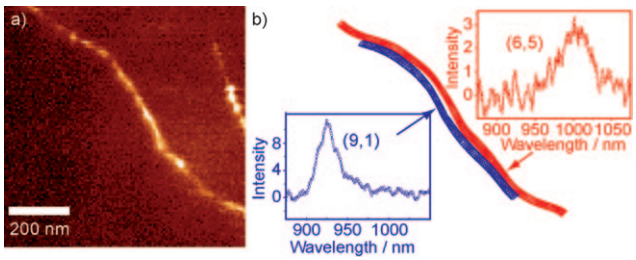

Figure 7. a) Near-field PL image of single-walled carbon nanotubes on mica formed by detecting the total PL between 860 and 1050 nm upon laser excitation at 632.8 nm and 5 μW. b) Near-field PL spectra recorded along the structure reveal that it is a bundle composed of two nanotubes with different emission energies. The structure parameters of both SWNTs were identified as (9,1) and (6,5) on the basis of the characteristic emission energies. In Ref. [125], the distance-dependent energy transfer from the (9,1) to the (6,5) nanotube was quantified with subnanometer accuracy.

7. Tip-Enhanced Raman Scattering

Raman scattering probes the vibrational spectrum of a sample and directly reflects its chemical composition and molecular structure. A main drawback of Raman scattering is the extremely low scattering cross-section, which is typically 14 orders of magnitude smaller than the cross-section of fluorescence. Clearly, both the high spatial resolution and signal enhancement provided by TENOM are needed for the detection of nanoscale sample volumes. In the following, selected examples are used to illustrate the possibilities and perspectives of tip-enhanced Raman scattering (TERS).

7.1. Signal Enhancement and Detection Sensitivity

A comprehensive list of reported enhancement factors (reaching up to 5×10^9) achieved in TERS is given in Ref. [10]. As discussed in Section 5, the measured relative signal enhancement—the ratio between enhanced near-field signal and background far-field signal—also reflects the different sample areas probed, and thus the field enhancement factors can not be quantified directly. In the derivation of these ratios, uniform sample properties, for example, uniform coverage for films and uniform signal characteristics along one-dimensional structures, are assumed. Figure 8 demonstrates the experimentally determined signal enhancement based on the Raman scattering signal detected from single-walled carbon nanotubes in the presence and absence of the tip. In this example, the signal enhancement was estimated to reach $M_{Raman} \approx (1–50) \times 10^7$, which corresponds to a field enhancement factor f between 60 and 150. The Raman intensity is recorded as a function of tip–sample distance d to demonstrate the confinement of the enhanced fields in the longitudinal direction.

Several recent publications have demonstrated that single molecules can be detected in tip-enhanced Raman measurements when the single molecules on metal substrates provide additional field enhancement.[54,128–132] The actual proof of single-molecule sensitivity is difficult and typically relies on the observation of spectral and intensity fluctuations that

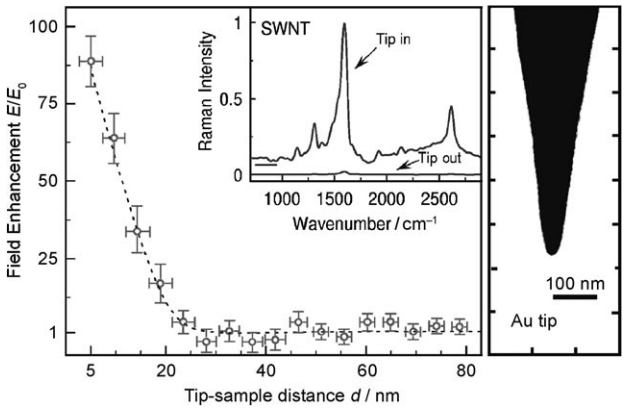

Figure 8. Left: Optical field enhancement versus tip–sample distance d derived from Raman scattering experiments. Inset: Corresponding Raman spectra for SWNTs on a Au surface with the tip at $d \approx 5$ nm ("tip in") and for a larger distance exceeding the near-field interaction length scale ("tip out"). Right: SEM image of a typical Au tip used for the experiments. Reprinted from Ref. [127], Copyright 2008, with permission from the Optical Society of America.

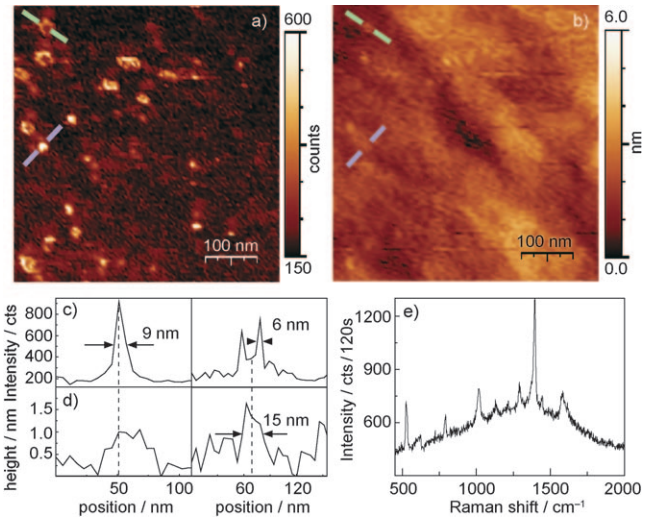

Figure 9. a) Near-field optical image of a smooth Au film covered with a layer of benzotriazole molecules (BTA), which shows the Raman signal of BTA on top of the photoluminescence signal of Au. b) The simultaneously recorded topography revealing only subnanometer variation in the height. The strongest near-field enhancement is observed for nanoscale protrusions. c,d) Intensity and height profiles over two small gold islands marked with lines. e) Raman spectrum detected at one of the bright features in (a). Reprinted from Ref. [60].

feature characteristic statistics upon lowering the sample concentration. Signal fluctuations could also result from temporal fluctuation of the enhancement efficiency for a superposition of molecules caused by physical/chemical changes of the adsorption sites and physical instabilities of the TERS tip during the experiment. Signal losses have also been attributed to tip-induced sample heating, which leads to weaker field enhancement by reducing the surface roughness as well as surface diffusion of adsorbates.[133] For extremely high field strength, photochemical modifications of the molecules need to be considered and distinguished in the spectroscopic data.[95,134] The detection of single molecules on a SERS substrate has been demonstrated unequivocally by using two isotopologues of rhodamine 6G that offer unique vibrational signatures.[135] Strong evidence for single-molecule detection in TERS has been presented very recently through the simultaneous observation of the sample coverage by STM and a linear dependence of the recorded signal amplitudes on the number of molecules within the optically probed area.[136]

7.2. Chemical Analysis of Surfaces

The chemical analysis of molecular species on surfaces is one of the main driving forces for the development of TERS, and holds great promise for applications in different areas such as catalysis. An example for near-field imaging with chemical contrast is shown in Figure 9.

A thin layer of benzotriazole molecules (BTA), a species that does not provide additional resonance enhancement at the laser excitation energy, has been imaged on a smooth gold film by a gold tip in the focus of a parabolic mirror objective. Here, the optical signal results from a superposition of the Raman scattering from BTA and the photoluminescence from the gold film. As described in Section 3 on field enhancement, additional signal amplification results from nanoscale protrusions within the metal film which lead to the very bright and highly localized features in the optical image (Figure 9a). In analogy to tip-enhanced fluorescence imaging (Section 6), the detected TERS signal will reflect the mutual orientation of the Raman scattering tensor and the enhanced fields. More specifically, the relative amplitudes of specific Raman lines can be utilized to extract information on the orientation and to monitor orientational mobility. Additional Raman lines, line splitting, or shifts can occur in the case of chemical binding of the molecule under study to the surface which can help to explore the details of the surface chemistry.

7.3. Biopolymers and Biosurfaces

DNA bases show characteristic Raman signatures, and the direct optical sequencing of DNA on substrates by using TERS has been a long-standing dream that has stimulated further development of the technique. Recent experiments on single RNA strands and picomole quantities of DNA bases indicate that this goal could be reachable.[129,137] The TER spectra shown in Figure 10 of different DNA nucleobases on Au(111) illustrates the enormous sensitivity achieved with TERS. Within the last few years, several TERS studies of biological samples have been reported, including the surfaces of ommatidial lens,[138] adenine nanocrystals,[139] cytochrome c,[140] and bacteria,[141] thus demonstrating the applicability of the technique.

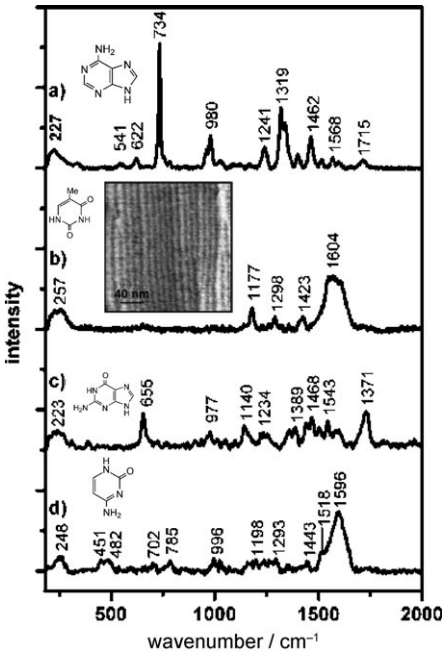

Figure 10. TER spectra (background-corrected) of DNA bases adsorbed on Au(111): a) adenine, b) thymine, c) guanine, and d) cytosine, normalized to a 1 s integration time at 2 mW incident power. The inset shows an STM image of a self-assembled thymine monolayer on Au(111). Reprinted from Ref. [129], Copyright 2007, with permission from the American Chemical Society.

7.4. Stress Imaging in Semiconductors

Since the length scales in semiconductor devices are constantly being reduced, the nanoscale imaging of dedicated stress in, for example, transistor structures, is of enormous technological relevance in regard to further progress in stress engineering.[10,142,143] Stress in silicon causes a shift of the Si-Si Raman band by about 4 cm^{-1} for 1 GPa of biaxial stress. For realistic (3D) stress states in actual device structures, a shift of about 1 cm^{-1} can be expected. The main challenge for Raman measurements on the nanoscale results from the far-field to near-field sample volume ratio, which makes the resulting variations in the surface signal extremely difficult to extract from the strong confocal background. Moreover, sample heating upon laser excitation also leads to significant Raman shifts of the order of 1 cm^{-1} per 50 K, thus making the identification of purely stress-induced features difficult.[144,145] The large reflectivity of silicon means that artefacts, in particular for periodic and layered structures, can result.[142] Different methods based on polarization filtering have been developed for enhancing the contrast and suppression of the background,[10,146,147] and TERS is very likely to become a useful tool for the investigation of semiconductor surfaces.

7.5. Raman Scattering of Carbon Nanotubes

The combination of the high spatial resolution and spectroscopic contrast achievable in TERS has been demonstrated for single-walled carbon nanotubes.[37,148–150] Raman scattering of SWNTs has been studied extensively,[118] and Raman enhancements of up to 10^{12} have been reported for nanotubes in contact with fractal silver colloidal clusters.[151] Figure 11 shows a near-field Raman image of a SWNT on

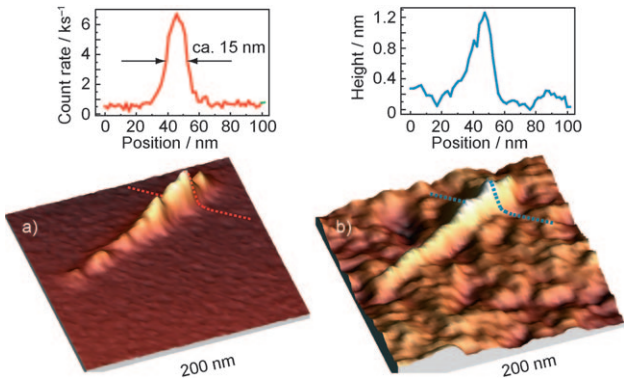

Figure 11. Simultaneously detected near-field Raman image (a) and topographic image (b) of a SWNT on glass. Scan area 0.2×0.2 μm^2. The Raman image was acquired by detecting the intensity of the Raman G band upon laser excitation at 633 nm.[118] The image acquisition time was about 20 minutes. The topography image reveals the roughness of the glass substrate. Shown above are cross-sections taken along the dashed lines in the respective images.

glass together with the simultaneously acquired topography image. The spatial resolution can be determined from the width of the signals presented as line scans to be about 15 nm. The sharpest images observed so far for glass substrates feature an optical resolution of about 10 nm, which is limited by the diameter of the tip.[150] In general, the measured optical width is smaller than the topographic width by about a factor of 1.3.[37,150] Although the topography signal of nanoscale objects will reproduce the tip shape, the fourth-order dependence of the Raman signal on the field enhancement will provide sharper optical images [Eq. (2)] (Section 4.1). The visualization of intramolecular junctions and defects along single nanotubes by TERS has been presented in Refs. [150,152].

Similar to the time-tagging approach used for fluorescence imaging (see Section 5), confocal background suppression can be achieved in TERS by correlating the detection event with the tapping mode oscillation.[55] Additional amplification is achieved in tip-enhanced coherent anti-Stokes Raman scattering (TE-CARS), as demonstrated in Ref. [153] for DNA networks. High spatial image contrast can also be achieved using other local tip-induced effects that do not rely on enhanced optical fields. Pressure-induced shifts of the Raman bands have been utilized in Ref. [154], and in Ref. [155] the chemical imaging of DNA bases is discussed based on the formation of local bonds with silver atoms at the tip.

8. Outlook

The results presented in this Review clearly demonstrate that TENOM has developed into a powerful and versatile tool. With this technique, the optical measurement of surfaces

with the highest spatial resolution to date have been achieved together with enormous signal enhancement. In addition, TENOM provides detailed structural information based on the observation of Raman scattering with ultrahigh detection sensitivity. A brief checklist for the applicability of TENOM to the characterization of a particular sample comprises the following points: 1) The surface can be characterized by AFM or STM, thus providing the basis for control over the tip–sample distance and the required nanoscale separation. 2) The optically active elements (e.g. Raman scatterers, fluorescent molecules) are close to the surface. 3) The sample shows a stable confocal microscopy signal. The far-field background and the favorable near-field to far-field ratio results in TENOM being particularly effective for 0D and 1D structures, such as point dipoles or wires. The imaging of bulk materials with small spectral contrast, however, remains challenging. Active research currently addresses this issue, and significant improvements in regard to signal enhancement and spatial resolution, eventually reaching a few nanometers, can also be expected within the next years.

Compared to far-field techniques, TENOM is likely to retain slightly higher spatial resolution, since it is limited essentially by the diameter of the tip end. Far-field techniques, however, provide much faster acquisition times than scanning-probe-based TENOM for the fluorescence imaging of high-quantum yield emitters. In fact, STED already permits video-rate fluorescence imaging.[21] Since the signal in TENOM results from electromagnetic near-field interactions between the probe and sample, the detected optical response can differ essentially from the far-field response. Tip-induced signal modifications need to be modeled and understood in detail to exploit this fact for sample characterization and to quantify the near-field optical contrast. For TENOM to develop into a standard procedure with broad applicability, the controlled, reproducible, and ideally parallel fabrication of tips with a high field enhancement factor needs to be achieved. This will be particularly challenging in the case of background-minimizing probes, such as TOA probes. Compact designs integrating optical microscopy and AFM/STM exist and can be optimized further to yield even more user-friendly systems. Besides providing a method for unprecedented sample analysis, TENOM is certainly a fascinating research field that helps to improve our understanding of near-field optical phenomena.

We thank our collaborators in this field of research. Projects were supported by the Deutsche Forschungsgemeinschaft (DFG-HA4405/3-1) and the Nanosystems Initiative Munich (NIM).

Received: April 6, 2008
Published online: September 22, 2008

[1] E. J. Sánchez, L. Novotny, X. S. Xie, *Phys. Rev. Lett.* **1999**, *82*, 4014 – 4017.
[2] S. Nie, S. R. Emory, *Science* **1997**, *275*, 1102 – 1106.
[3] J. Y. P. Butter, B. Hecht, B. R. Crenshaw, C. Weder, *J. Chem. Phys.* **2006**, *125*, 154710.
[4] P. Kukura, M. Celebrano, A. Renn, V. Sandoghdar, *Condens. Matter* **2008**, *arXiv:*, 0802.1206v1.
[5] D. W. Pohl, W. Denk, M. Lanz, *Appl. Phys. Lett.* **1984**, *44*, 651 – 653.
[6] A. Lewis, M. Isaacson, A. Harootunian, A. Muray, *Ultramicroscopy* **1984**, *13*, 227 – 231.
[7] D. W. Pohl, *Philos. Trans. R. Soc. London Ser. A* **2004**, *362*, 701 – 717.
[8] L. Novotny, *Progress in Optics*, *Vol. 50* (Ed.: E. Wolf), Elsevier, Amsterdam, **2007**, pp. 137 – 184.
[9] L. Novotny, B. Hecht, *Principles of Nano-Optics*, Cambridge University Press, Cambridge, **2006**.
[10] "Tip enhancement": *Advances in Nano-Optics and Nano-Photonics* (Eds.: S. Kawata, V. M. Shalaev), Elsevier, Amsterdam, **2007**.
[11] A. Hartschuh, M. R. Beversluis, A. Bouhelier, L. Novotny, *Philos. Trans. R. Soc. London Ser. A* **2004**, *362*, 807 – 819.
[12] A. Bouhelier, *Micr. Res. Techn.* **2006**, *69*, 563 – 579.
[13] E. Abbe, *Arch. Mikrosk. Anat.* **1873**, *9*, 413.
[14] L. Rayleigh, *Philos. Mag.* **1879**, *8*, 261 – 274.
[15] M. Born, E. Wolf, *Principles of Optics*, 6th ed., Pergamon, Oxford, **1970**.
[16] M. Dyba, S. Hell, *Phys. Rev. Lett.* **2002**, *88*, 163901.
[17] R. J. Kittel, C. Wichmann, T. M. Rasse, W. Fouquet, M. Schmidt, A. Schmid, D. A. Wagh, C. Pawlu, R. R. Kellner, K. I. Willig, S. Hell, E. Buchner, M. Heckmann, S. J. Sigrist, *Science* **2006**, *312*, 1051 – 1054.
[18] E. Betzig, G. H. Patterson, R. Sougrat, O. W. Lindwasser, S. Olenych, J. S. Bonifacino, M. W. Davidson, J. Lippincott-Schwartz, H. F. Hess, *Science* **2006**, *313*, 1642 – 1645.
[19] M. J. Rust, M. Bates, X. Zhuang, *Nat. Methods* **2006**, *3*, 793 – 796.
[20] A. Yildiz, M. Tomishige, R. D. Vale, P. R. Selvin, *Science* **2004**, *303*, 676 – 678.
[21] S. Hell, *Science* **2007**, *316*, 1153 – 1158.
[22] B. Huang, W. Wang, M. Bates, X. Zhuang, *Science* **2008**, *319*, 810 – 813.
[23] N. Anderson, P. Anger, A. Hartschuh, L. Novotny, *Nano Lett.* **2006**, *6*, 744 – 749.
[24] E. Betzig, J. K. Trautman, *Science* **1992**, *257*, 189 – 195.
[25] B. Dunn, *Chem. Rev.* **1999**, *99*, 2891 – 2928.
[26] L. Novotny, D. W. Pohl, *NATO Adv. Study Inst. Ser. Ser. E* **1995**, *184*, 21 – 33.
[27] J. Wessel, *J. Opt. Soc. Am. B* **1985**, *2*, 1538 – 1541.
[28] B. Knoll, F. Keilmann, *Nature* **1999**, *399*, 134 – 137.
[29] R. Hillenbrand, T. Taubner, F. Keilmann, *Nature* **2002**, *418*, 159 – 162.
[30] F. Keilmann, R. Hillenbrand, *Philos. Trans. R. Soc. London Ser. A* **2004**, *362*, 787 – 805.
[31] A. Zayats, V. Sandoghdar, *Opt. Commun.* **2000**, *178*, 245 – 249.
[32] A. V. Zayats, I. I. Smolyaninov, *Philos. Trans. R. Soc. London Ser. A* **2004**, *362*, 843 – 860.
[33] A. Bouhelier, M. Beversluis, A. Hartschuh, L. Novotny, *Phys. Rev. Lett.* **2003**, *90*, 013903.
[34] M. Danckwerts, L. Novotny, *Phys. Rev. Lett.* **2007**, *98*, 026104.
[35] S. M. Stöckle, Y. D. Suh, V. Deckert, R. Zenobi, *Chem. Phys. Lett.* **2000**, *318*, 131 – 136.
[36] N. Hayazawa, Y. Inouye, Z. Sekkat, S. Kawata, *Chem. Phys. Lett.* **2001**, *335*, 369 – 374.
[37] A. Hartschuh, E. J. Sánchez, X. S. Xie, L. Novotny, *Phys. Rev. Lett.* **2003**, *90*, 095503.
[38] L. Novotny, R. X. Bian, X. S. Xie, *Phys. Rev. Lett.* **1997**, *79*, 645 – 648.
[39] R. Kappeler, D. Erni, C. Xudong, L. Novotny, *J. Comput. Theor. Nanosci.* **2007**, *4*, 686 – 691.
[40] C. C. Neascu, G. A. Steudle, M. B. Raschke, *Appl. Phys. B* **2005**, *80*, 295 – 300.

[41] Y. C. Martin, H. F. Hamann, H. K. Wickramasinghe, *J. Appl. Phys.* **2001**, *89*, 5774 – 5778.
[42] J. T. I. Krug, E. J. Sánchez, X. S. Xie, *J. Chem. Phys.* **2002**, *116*, 10895 – 10901.
[43] L. Novotny, *Phys. Rev. Lett.* **2007**, *98*, 266802.
[44] P. Mühlschlegel, H.-J. Eisler, B. Hecht, D. W. Pohl, *Science* **2005**, *308*, 1607 – 1609.
[45] T. Grosges, A. Vial, D. Barchiesi, *Opt. Express* **2005**, *13*, 8483 – 8497.
[46] G. A. Baker, D. S. Moore, *Anal. Bioanal. Chem.* **2005**, *382*, 1751 – 1770.
[47] R. M. Bakker, H.-K. Yuan, Z. Liu, V. P. Drachev, A. V. Kildishev, V. M. Shalaev, R. H. Pedersen, S. Gresillon, A. Boltasseva, *Appl. Phys. Lett.* **2008**, *92*, 043101.
[48] P. Olk, J. Renger, T. Härtling, M. T. Wenzel, L. M. Eng, *Nano Lett.* **2007**, *7*, 1736 – 1740.
[49] H. Xu, E. J. Bjerneld, M. Käll, L. Börjesson, *Phys. Rev. Lett.* **1999**, *83*, 4357 – 4360.
[50] O. L. Muskens, V. Giannini, J. A. Sánchez-Gil, J. G. Rivas, *Nano Lett.* **2007**, *7*, 2871 – 2875.
[51] L. Rogobete, F. Kaminski, M. Agio, V. Sandoghdar, *Opt. Express* **2007**, *32*, 1623 – 1625.
[52] A. Alù, N. Engheta, *Nat. Photonics* **2008**, *2*, 307 – 310.
[53] I. Notingher, A. Elfick, *J. Phys. Chem. B* **2005**, *109*, 15699 – 15706.
[54] C. C. Neacsu, J. Dreyer, N. Behr, M. B. Raschke, *Phys. Rev. B* **2006**, *73*, 193406.
[55] T. Yano, T. Ichimura, A. Taguchi, N. Hayazawa, P. Verma, Y. Inouye, S. Kawata, *Appl. Phys. Lett.* **2007**, *91*, 121101.
[56] N. Hayazawa, H. Ishitobi, A. Taguchi, A. Tarun, K. Ikeda, S. Kawata, *Jpn. J. Appl. Phys.* **2007**, *46*, 7995 – 7999.
[57] T. Kalkbrenner, U. Hakanson, A. Schädle, S. Burger, C. Henkel, V. Sandoghdar, *Phys. Rev. Lett.* **2005**, *95*, 200801.
[58] B. Pettinger, K. F. Domke, D. Zhang, R. Schuster, G. Ertl, *Phys. Rev. B* **2007**, *76*, 113409.
[59] B. S. Yeo, T. Schmid, W. Zhang, R. Zenobi, *Anal. Bioanal. Chem.* **2007**, *387*, 2655 – 2662.
[60] M. Sackrow, C. Stanciu, M. A. Lieb, A. J. Meixner, *ChemPhysChem* **2008**, *9*, 316 – 320.
[61] W. Zhang, X. Cui, B. S. Yeo, T. Schmid, C. Hafner, R. Zenobi, *Nano Lett.* **2007**, *7*, 1401 – 1405.
[62] B. Hecht, H. Bielefeldt, Y. Inouye, D. W. Pohl, L. Novotny, *J. Appl. Phys.* **1997**, *81*, 2492 – 2498.
[63] S. I. Bozhevolnyi, *J. Opt. Soc. Am. B* **1997**, *14*, 2254 – 2259.
[64] M. I. Stockman, S. V. Faleev, D. J. Bergman, *Phys. Rev. Lett.* **2002**, *88*, 067402.
[65] T. Brixner, F. J. García de Abajo, J. Schneider, W. Pfeiffer, *Phys. Rev. Lett.* **2005**, *95*, 093901.
[66] M. I. Stockman, M. F. Kling, U. Kleineberg, F. Krausz, *Nat. Photonics* **2007**, *1*, 539 – 544.
[67] M. Aeschlimann, M. Bauer, D. Bayer, T. Brixner, F. J. García de Abajo, W. Pfeiffer, M. Rohmer, C. Spindler, F. Steeb, *Nature* **2007**, *446*, 301 – 304.
[68] L. Novotny, S. Stranick, *Annu. Rev. Phys. Chem.* **2006**, *57*, 303 – 331.
[69] J. Nelayah, M. Kociak, O. Stéphan, F. J. García de Abajo, M. Tencé, L. Henrard, D. Taverna, I. Pastoriza-Santos, L. M. Liz-Marzán, C. Colliex, *Nat. Phys.* **2007**, *3*, 348 – 353.
[70] E. M. Purcell, *Phys. Rev.* **1946**, *69*, 681.
[71] M. Thomas, R. Carminati, J. R. Arias-Gonzalez, J.-J. Greffet, *Appl. Phys. Lett.* **2004**, *85*, 3863 – 3865.
[72] H. Xu, J. Aizpurua, M. Käll, P. Apell, *Phys. Rev. E* **2000**, *62*, 4318 – 4323.
[73] A. Hartschuh, H. Qian, A. J. Meixner, N. Anderson, L. Novotny, *Nano Lett.* **2005**, *5*, 2310 – 2313.
[74] K. Aslan, I. Gryczynski, J. Malicka, E. Matveea, J. R. Lakowicz, C. D. Geddes, *Anal. Biotechnol.* **2005**, *16*, 55 – 62.
[75] R. R. Chance, A. Prock, R. Silbey, *J. Chem. Phys.* **1974**, *60*, 2744 – 2748.
[76] W. L. Barnes, *J. Mod. Opt.* **1998**, *45*, 661 – 699.
[77] A. Bek, R. Jansen, M. Ringler, S. Mayilo, T. A. Klar, J. Feldmann, *Nano Lett.* **2005**, *5*, 585 – 589.
[78] R. Carminati, J. J. Greffet, C. Henkel, J. M. Vigoureux, *Opt. Express* **2006**, *261*, 368 – 375.
[79] N. A. Issa, R. Guckenberger, *Opt. Express* **2007**, *15*, 12131 – 12144.
[80] G. Baffou, C. Girard, E. Dujardin, G. Colas des Francs, O. J. F. Martin, *Phys. Rev. B* **2008**, *77*, 121101.
[81] J. N. Farahani, D. W. Pohl, H.-J. Eisler, B. Hecht, *Phys. Rev. Lett.* **2005**, *95*, 017402.
[82] P. Anger, P. Bharadwaj, L. Novotny, *Phys. Rev. Lett.* **2006**, *96*, 113002.
[83] S. Kühn, U. Hakanson, L. Rogobete, V. Sandoghdar, *Phys. Rev. Lett.* **2006**, *97*, 017402.
[84] P. Bharadwaj, P. Anger, L. Novotny, *Nanotechnology* **2007**, *18*, 044017.
[85] R. Eckel, V. Walhorn, C. Pelargus, J. Martini, J. Enderlein, T. Nann, D. Anselmetti, R. Ros, *Small* **2007**, *3*, 44 – 49.
[86] M. Ringler, A. Schwemer, M. Wunderlich, A. Nichtl, K. Kürzinger, T. A. Klar, J. Feldmann, *Phys. Rev. Lett.* **2008**, *100*, 203002.
[87] T. H. Taminniau, F. D. Stefani, F. B. Segerink, N. F. van Hulst, *Nat. Photonics* **2008**, *2*, 234 – 237.
[88] M. Stavola, D. L. Dexter, R. S. Knox, *Phys. Rev. B* **1985**, *31*, 2277 – 2289.
[89] J. Azoulay, A. Débarre, A. Richard, P. Tchénio, *Europhys. Lett.* **2000**, *51*, 374 – 380.
[90] J. R. Zurita-Sánchez, L. Novotny, *J. Opt. Soc. Am. B* **2002**, *19*, 1355 – 1362.
[91] U. Hohenester, G. Goldoni, E. Molinari, *Appl. Phys. Lett.* **2004**, *84*, 3963 – 3965.
[92] U. Hohenester, G. Goldoni, E. Molinari, *Phys. Rev. Lett.* **2005**, *95*, 216802.
[93] E. J. Ayars, H. D. Hallen, C. L. Jahncke, *Phys. Rev. Lett.* **2000**, *85*, 4180 – 4183.
[94] K. Karrai, R. D. Grober, *Appl. Phys. Lett.* **1995**, *66*, 1842 – 1844.
[95] B. Pettinger, B. Ren, G. Picardi, R. Schuster, G. Ertl, *Phys. Rev. Lett.* **2004**, *92*, 096101.
[96] T. Kalkbrenner, M. Ramstein, J. Mlynek, V. Sandoghdar, *J. Microsc.* **2001**, *202*, 72 – 76.
[97] I. Barsegova, A. Lewis, A. Khatchatouriants, A. Manevitch, A. Ignatov, N. Axelrod, C. Sukenik, *Appl. Phys. Lett.* **2002**, *81*, 3461 – 3463.
[98] I. U. Vakarelski, K. Higashitani, *Langmuir* **2006**, *22*, 2931 – 2934.
[99] P. J. Schuck, D. P. Fromm, A. Sundaramurthy, G. S. Kino, W. E. Moerner, *Phys. Rev. Lett.* **2005**, *94*, 017402.
[100] J. N. Farahani, H.-J. Eisler, D. W. Pohl, M. Pavius, P. Flückiger, B. Gasser, P. Hecht, *Nanotechnology* **2007**, *18*, 125506.
[101] L. Novotny, E. J. Sánchez, X. S. Xie, *Ultramicroscopy* **1998**, *71*, 21 – 29.
[102] S. Quabis, R. Dorn, O. Glöckl, M. Eberler, G. Leuchs, *Opt. Commun.* **2000**, *179*, 1 – 7.
[103] A. Lieb, A. J. Meixner, *Opt. Express* **2001**, *8*, 458 – 474.
[104] J. Steidtner, B. Pettinger, *Rev. Sci. Instrum.* **2007**, *78*, 103104.
[105] Z. Ma, J. M. Gerton, L. A. Wade, S. R. Quake, *Phys. Rev. Lett.* **2006**, *97*, 260801.
[106] H. G. Frey, F. Keilmann, A. Kriele, R. Guckenberger, *Appl. Phys. Lett.* **2002**, *81*, 5300 – 5320.
[107] H. G. Frey, S. Witt, K. Felderer, R. Guckenberger, *Phys. Rev. Lett.* **2004**, *93*, 200801.
[108] T. H. Taminiau, R. J. Moerland, F. B. Segerink, L. Kuipers, N. F. van Hulst, *Nano Lett.* **2007**, *7*, 28 – 33.

[109] C. Ropers, C. C. Neacsu, T. Elsaesser, M. Albrecht, M. B. Raschke, C. Lienau, *Nano Lett.* **2007**, *7*, 2784 – 2788.
[110] J. M. Eckert, R. Freyland, H. Gersen, H. Heinzelmann, G. Schürmann, W. Noell, U. Staufer, N. F. de Rooij, *Appl. Phys. Lett.* **2000**, *77*, 3695 – 3697.
[111] A. Bouhelier, J. Renger, M. R. Beversluis, L. Novotny, *J. Microsc.* **2003**, *210*, 220 – 224.
[112] F. M. Huang, F. Festy, D. Richards, *Appl. Phys. Lett.* **2005**, *87*, 183101.
[113] H. Frey, C. Bolwien, A. Brandenburg, R. Ros, D. Anselmetti, *Nanotechnology* **2006**, *17*, 3105 – 3110.
[114] J. Seelig, K. Leslie, S. Renn, A. Kühn, V. Jacobsen, M. van de Corput, C. Wyman, V. Sandoghdar, *Nano Lett.* **2007**, *7*, 685 – 689.
[115] S. Kühn, V. Sandoghdar, *Appl. Phys. B* **2006**, *84*, 211 – 217.
[116] A. Kramer, W. Trabesinger, B. Hecht, U. P. Wild, *Appl. Phys. Lett.* **2002**, *80*, 1652 – 1654.
[117] C. Höppener, L. Novotny, *Nano Lett.* **2008**, *8*, 642 – 646.
[118] "Carbon Nanotubes": *Topics in Applied Physics*, *Vol. 111* (Eds.: A. Jorio, M. S. Dresselhaus, G. Dresselhaus), Springer, Berlin, **2008**.
[119] K. Welsher, Z. Liu, D. Daranciang, H. Dai, *Nano Lett.* **2008**, *8*, 586 – 590.
[120] F. Wang, G. Dukovic, L. E. Brus, T. F. Heinz, *Phys. Rev. Lett.* **2004**, *92*, 177401.
[121] M. J. O'Connell, S. M. Bachilo, C. B. Huffman, V. C. Moore, M. S. Strano, E. H. Haroz, K. L. Rialon, P. J. Boul, W. H. Noon, C. Kittrell, J. Ma, R. H. Hauge, R. B. Weisman, R. Smalley, *Science* **2002**, *297*, 593 – 596.
[122] Z. Zhu, J. Crochet, M. S. Arnold, M. C. Hersam, H. Ulbricht, D. Resasco, T. Hertel, *J. Phys. Chem. C* **2007**, *111*, 3831 – 3835.
[123] A. Hartschuh, H. N. Pedrosa, L. Novotny, T. D. Krauss, *Science* **2003**, *301*, 1354 – 1356.
[124] A. Hagen, M. Steiner, M. B. Raschke, C. Lienau, T. Hertel, H. Qian, A. J. Meixner, A. Hartschuh, *Phys. Rev. Lett.* **2005**, *95*, 197401.
[125] H. Qian, C. Georgi, N. Anderson, A. A. Green, M. C. Hersam, L. Novotny, A. Hartschuh, *Nano Lett.* **2008**, *8*, 1363 – 1367.
[126] H. Qian, T. Gokus, N. Anderson, A. J. Novotny, L. Meixner, A. Hartschuh, *Phys. Status Solidi B* **2006**, *243*, 3146 – 3150.
[127] R. M. Roth, N. C. Panoiu, M. M. Adams, R. M. Osgood, Jr., C. C. Neacsu, M. B. Raschke, *Opt. Express* **2006**, *14*, 2921 – 2931.
[128] W. Zhang, B. S. Yeo, T. Schmid, R. Zenobi, *J. Phys. Chem. C* **2007**, *111*, 1733 – 1738.
[129] K. F. Domke, D. Zhang, B. Pettinger, *J. Am. Chem. Soc.* **2007**, *129*, 6708 – 6709.
[130] K. F. Domke, D. Zhang, B. Pettinger, *J. Am. Chem. Soc.* **2006**, *128*, 14721 – 14727.
[131] C. C. Neacsu, J. Dreyer, N. Behr, M. B. Raschke, *Phys. Rev. B* **2007**, *75*, 236402.
[132] D. R. Ward, N. J. Halas, J. W. Ciszek, J. M. Tour, Y. Wu, P. Nordlander, D. Natelson, *Nano Lett.* **2008**, *8*, 919 – 924.
[133] W. Zhang, T. Schmid, B. S. Yeo, R. Zenobi, *J. Phys. Chem. C* **2008**, *112*, 2104 – 2108.
[134] K. F. Domke, D. Zhang, B. Pettinger, *J. Phys. Chem. C* **2007**, *111*, 8611 – 8616.
[135] J. A. Dieringer, R. B. Lettan II, K. A. Scheidt, R. P. Van Duyne, *J. Am. Chem. Soc.* **2007**, *129*, 16249 – 16256.
[136] J. Steidtner, B. Pettinger, *Phys. Rev. Lett.* **2008**, *100*, 236101.
[137] E. Bailo, V. Deckert, *Angew. Chem.* **2008**, *120*, 1682 – 1685; *Angew. Chem. Int. Ed.* **2008**, *47*, 1658 – 1661.
[138] M. S. Anderson, S. D. Gaimari, *J. Struct. Biol.* **2003**, *142*, 364 – 368.
[139] H. Watanabe, Y. Ishida, N. Hayazawa, Y. Inouye, S. Kawata, *Phys. Rev. B* **2004**, *69*, 155418.
[140] B. S. Yeo, S. Mädler, T. Schmid, W. Zhang, R. Zenobi, *J. Phys. Chem. C* **2008**, *112*, 4867 – 4873.
[141] U. Neugebauer, M. Rösch, M. Schmitt, J. Popp, C. Julien, A. Rasmussen, C. Budich, V. Deckert, *ChemPhysChem* **2006**, *7*, 1428 – 1430.
[142] C. Georgi, M. Hecker, E. Zschech, *Appl. Phys. Lett.* **2007**, *90*, 171102.
[143] A. Tarun, N. Hayazawa, M. Motohashi, S. Kawata, *Rev. Sci. Instrum.* **2007**, *79*, 913706.
[144] T. R. Hart, R. L. Aggarwal, B. Lax, *Phys. Rev. B* **1970**, *1*, 638 – 642.
[145] C. Georgi, M. Hecker, E. Zschech, *J. Appl. Phys.* **2007**, *101*, 123104.
[146] R. Ossikovski, Q. Nguyen, G. Picardi, *Phys. Rev. B* **2007**, *75*, 045412.
[147] M. Motohashi, N. Hayazawa, A. Tarun, S. Kawata, *J. Appl. Phys.* **2008**, *103*, 034309.
[148] N. Hayazawa, T. Yano, H. Watanabe, Y. Inouye, S. Kawata, *Chem. Phys. Lett.* **2003**, *376*, 174 – 180.
[149] A. Hartschuh, A. J. Meixner, L. Novotny, *AIP Conf. Proc.* **2004**, *723*, 63 – 66.
[150] N. Anderson, A. Hartschuh, L. Novotny, *J. Am. Chem. Soc.* **2005**, *127*, 2533 – 2537.
[151] K. Kneipp, H. Kneipp, P. Corio, S. D. Brown, K. Shafer, J. Motz, L. T. Perelman, E. B. Hanlon, A. Marucci, G. Dresselhaus, M. S. Dresselhaus, *Phys. Rev. Lett.* **2000**, *84*, 3470.
[152] N. Anderson, A. Hartschuh, L. Novotny, *Nano Lett.* **2007**, *7*, 577 – 582.
[153] T. Ichimura, N. Hayazawa, M. Hashimoto, Y. Inouye, S. Kawata, *Phys. Rev. Lett.* **2004**, *92*, 220801.
[154] T. Yano, Y. Inouye, S. Kawata, *Nano Lett.* **2006**, *6*, 1269 – 1273.
[155] N. Hayazawa, H. Watanabe, Y. Saito, S. Kawata, *J. Chem. Phys.* **2006**, *125*, 244706.